DOI: 10.1002/chem.200700226

Optoelectronic logic devices based on nanocrystalline TiO_2

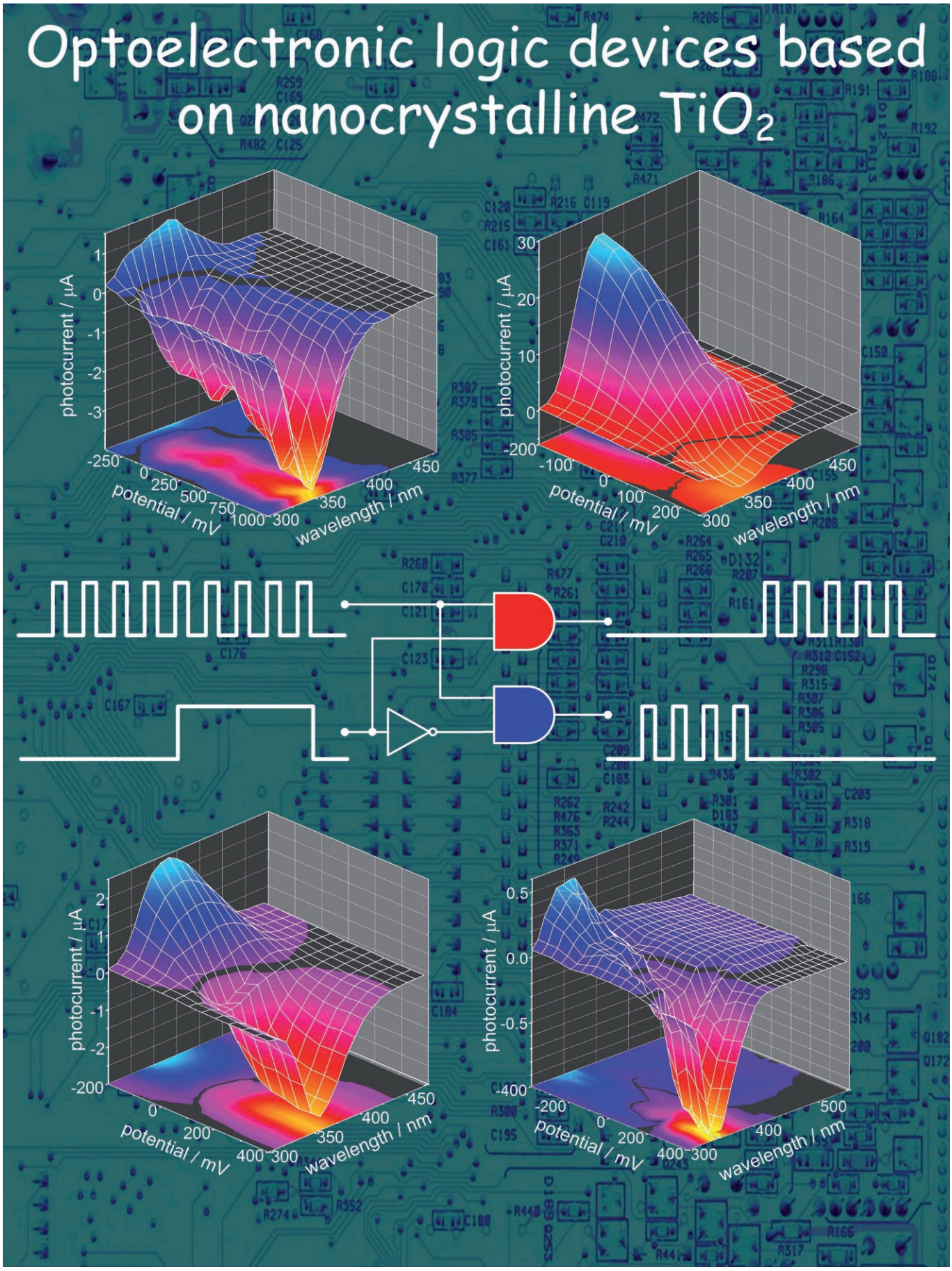

Photosensitization and the Photocurrent Switching Effect in Nanocrystalline Titanium Dioxide Functionalized with Iron(II) Complexes: A Comparative Study

Wojciech Macyk, Grażyna Stochel, and Konrad Szaciłowski*[a]

Abstract: Selected iron(II) complexes (ferrocene, ferrocenylboronic acid, hexacyanoferrate(II)) have been used as photosensitizers of titanium dioxide. Various types of electronic interactions between the surface complex and the semiconducting support are reflected in different yields of photocurrent generated upon visible-light irradiation and different efficiencies of the photosensitization effect. The studied systems, showing the photocurrent switching upon changes of electrode potential and energy of photons (the PEPS effect), are good models of simple photoelectrochemical logic devices. The mechanism of photosensitization and photocurrent switching is discussed with respect to the type of surface-complex–support interaction. Quantum-mechanical calculations support the proposed mechanisms.

Keywords: electrochemistry · electron transfer · photochemistry · semiconductors · titanium dioxide

Introduction

Photoinduced, interfacial electron-transfer processes are crucial for solar cells, photonic switches, logic gates, and semiconductor photocatalysis. These processes are the last step of photophysical processes within semiconductor crystals that occur upon light absorption. In the primary step, excitons are generated, which in turn can annihilate (on radiative or thermal pathways) or dissociate yielding mobile electrons in the conduction band (CB) and holes in the valence band (VB), respectively. The further fate of the charge carriers depends on the concentration of bulk and surface defects acting as charge traps. Bulk doping and surface modification, along with photosensitization supply easily accessible, redox active sites that can participate in electron-transfer processes. Visible-light photosensitization also consists of photoinduced electron transfer. It can be achieved by four main approaches: 1) bulk doping, 2) surface modification, 3) formation of composite semiconductors,[1–7] and 4) metal-semiconductor composites.[8–13]

Bulk doping results in the formation of intra-band-gap donor or acceptor levels that render the effective band gap smaller (Figure 1a). The modification usually involves introduction of p-block (N,[14–17] C,[18–20] S,[20,21] Cl, Br,[22] I,[23] Pb[24]), d-block (V,[25] Cr,[26,27] Au, Rh, Ni,[28] Pt,[28–32] etc.) or f-block (Eu, Pr, Yb,[33] Ce,[34] Nd[35] etc.) elements into TiO_2 (or other wide-band-gap semiconductors) matrix. Surface modification, in turn, involves formation of covalent or ionic bonds between a semiconductor surface and chromophoric molecules or formation of chromophoric surface species upon interaction with chromogenic molecules. In the first

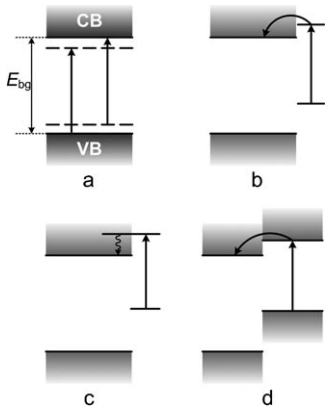

Figure 1. Modes of band-gap "narrowing": a) bulk doping resulting in formation of acceptor or donor levels; b) photosensitization with organic or inorganic chromophores chemisorbed onto semiconductor surface; c) formation of surface complexes exhibiting MMCT or LMCT transitions; d) formation of composite semiconductors. E_{bg} stands for the band-gap energy.

[a] Dr. W. Macyk, Prof. G. Stochel, Dr. K. Szaciłowski
Centrum Nanochemii Nieorganicznej, Wydział Chemii
Uniwersytet Jagielloński, ul. Romana Ingardena 3
30–060 Kraków (Poland)
Fax: (+48) 12-634-0515
E-mail: szacilow@chemia.uj.edu.pl

case diverse organic dyes (porphyrins,[36–40] phthalocyanines,[41–45] thiacarbocyanine dyes,[46,47] various natural dyes[48–56]) and metal complexes[49] undergo photoexcitation with visible light and inject electrons into the conduction band (Figure 1b). Chemisorption of chromogenic molecules onto the TiO_2 surface results in formation of ligand-to-metal or metal-to-metal charge transfer (LMCT and MMCT, respectively; more precisely referred to as ligand-to-particle or metal-to-particle charge transfer; LPCT and MPCT) involving surface Ti^{IV} ions and surface-bound ligands or transition-metal complexes, respectively. Photoexcitation of these systems results in a direct electron injection into the CB as a consequence of photon absorption (Figure 1c). Composite semiconductors are formed when TiO_2 particles interact with particles (or are covered with layers) of semiconductors of smaller band-gap and different band-edge potentials. Visible-light irradiation leads to charge separation only in the smaller band-gap semiconductor and subsequently electrons can be injected into the CB of TiO_2 (Figure 1d). This process results not only in photosensitization, but also in more efficient charge separation and suppression of recombination processes. Similar processes take place upon excitation of metal nanoparticles within their plasmon resonance bands.

The most commonly used technique of TiO_2 photosensitization is surface modification. The simple quantum-chemical description of photophysical processes involved in surface-modified metals and semiconductors was given recently by Galperin and Nitzan.[57–60] Properties of the surface-modified semiconductor can be derived from an interaction between isolated electronic levels of the surface molecules (especially HOMO and LUMO orbitals) and the electronic continuum of semiconductor under the influence of a radiation field. The total Hamiltonian of the system can be thus formulated as a sum of Hamiltonians for all the components of the system ($\hat{H}_0$) and a coupling operator including all the physical processes of interest ($\hat{V}$) [Eq. (1)]:

Abstract in Polish: *Wybrane kompleksy żelaza(II) (ferrocen, kwas ferrocenyloboronowy i heksacyjanożelazian(II)) zostały użyte jako fotosensybilizatory dwutlenku tytanu. Różne typy oddziaływań elektronowych pomiędzy kompleksami powierzchniowymi a podłożem półprzewodnikowym znajdują odbicie w różnych wydajnościach generacji fotoprądu i różnym stopniu fotosensybilizacji materiałów na światło widzialne. Wszystkie badane układy wykazują efekt fotoelektrochemicznego przełączenia fotoprądu na skutek zmian potencjału fotoelektrody i zmian długości fali światła padającego (efekt PEPS), dlatego też stanowią bardzo dobre modele prostych przełączników fotoelektrochemicznych. Niniejsza praca szczegółowo określa mechanizm fotosensybilizacji i przełączenia fotoprądu na podstawie analizy oddziaływań pomiędzy kompleksem a powierzchnią półprzewodnika. Obliczenia kwantowo-mechaniczne potwierdzają postulowany mechanizm.*

$$\hat{H} = \hat{H}_0 + \hat{V} \quad (1)$$

The $\hat{H}_0$ Hamiltonian is simply a sum of the Hamiltonians of individual components of the system [Eq. (2)], in which $\hat{H}_M$, $\hat{H}_S$, and $\hat{H}_R$ are the Hamiltonians for the isolated molecule, the semiconducting substrate, and the radiation field, respectively. The coupling operator in turn can be formulated as Equation (3).

$$\hat{H}_0 = \hat{H}_M + \hat{H}_S + \hat{H}_R \quad (2)$$

$$\hat{V} = \hat{V}_{ET} + \hat{V}_{DC} + \hat{V}_{RM} + \hat{V}_{RS} + \hat{V}_{RMS} \quad (3)$$

The coupling operator includes terms corresponding to the following processes: electron-transfer coupling between each isolated molecular electronic state of the molecule and the electronic continuum of the semiconductor ($\hat{V}_{ET}$); dipole-induced dipole coupling (energy-transfer), which describes interaction of an excited molecule and the dielectric response of the substrate ($\hat{V}_{DC}$); molecule-radiation-field coupling ($\hat{V}_{RM}$), describing light absorption by the isolated molecule; substrate-radiation-field coupling ($\hat{V}_{RS}$) depicting optical properties of the semiconductor; and molecule/substrate-radiation-field coupling ($\hat{V}_{RMS}$), which describes a direct optical excitation between the substrate electronic continuum and a molecular electronic state or vice versa. Photosensitization by organic chromophores or transition-metal complexes chemisorbed onto the semiconductor surface can be in most cases described simply by the combination of $\hat{V}_{RM}$ and $\hat{V}_{ET}$ terms: energy quanta are absorbed by the chromophore and electrons from its excited state are injected into the conduction band of the semiconductor (cf. Figure 1c). On the other hand the direct photoinduced electron transfer from the surface bound molecule described by the $\hat{V}_{RMS}$ term (cf. Figure 1d) was reported only for cyanoferrate-[61–72] and catechol-modified[73] titanium dioxide.

The above-mentioned theoretical background shows that irrespective of the chemical nature of the photosensitizer and its binding mode to the semiconductor surface, one should consider two main ways of populating the semiconductor CB: direct and indirect. Direct processes include VB→CB excitations, photosensitization through bulk doping ($\hat{V}_{RS}$-driven processes) and photophysical processes involving the $\hat{V}_{RMS}$ term. Indirect processes, in turn, involve excitation of the surface and a subsequent electron-transfer reactions ($\hat{V}_{RM}+\hat{V}_{ET}$).

The pathway of the photoinduced electron transfer within the semiconductor–photosensitizer system depends thus strongly on the binding mode of the modifier to the semiconductor particle, that is, on the strength of the electronic coupling ($\hat{V}_{ET}$). In this respect, studies on the correlation between spectral, electrochemical, and photoelectrochemical properties of nanocrystalline TiO_2 with various photo- and redox-active molecules are very important. This work presents a comparative study on photoelectrochemistry of titanium dioxide modified noncovalently and covalently with various iron(II) complexes: ferrocene, ferrocenylboronic acid,

and hexacyanoferrate. The first complex is attached noncovalently, the second covalently by means of a σ-linker, while the last one covalently through a π-linker. Similarities and differences of photoelectrochemical response of these materials are related to quantum-chemical modeling at B3PW91/6–311++G(d,p) level of theory.

Results and Discussion

Photosensitizer–support interaction: Impregnation of commercially available TiO_2 (P25, Degussa) with solutions of iron complexes resulted in formation of colored materials: ferrocene-modified TiO_2 (Fc@TiO_2), ferrocenylboronic acid modified TiO_2 (FcB@TiO_2) and titanium dioxide modified with hexacyanoferrate(II) ($[Fe(CN)_6]^{4-}$@TiO_2). Their electronic spectra are presented in Figure 2. The onsets of visible-light absorptions are localized between 600 and 700 nm in all the studied cases. The complexes show a rather small influence on band-gap energy of the titanium dioxide support, which can be estimated to be equal to 3.25 eV. The spectral features of Fc@TiO_2 are reminiscent of those of the individual components of this material (Figure 2). Only a slight hypsochromic shift of the ferrocene absorption band (by ca. 5 nm) can be observed. This is consistent with a negligibly weak electronic coupling between ferrocene and titanium dioxide crystals, which results from the lack of any covalent bonding. A broad absorption shoulder of a low intensity can be observed in the case of FcB@TiO_2. The diffuse reflectance spectrum of the FcB@TiO_2 material does not resemble the sum of the components. The spectrum contains an absorption edge characteristic for semiconductors and a weak, but broad, featureless band between 400 and 660 nm. This absorption can be tentatively attributed to the charge-transfer transition similar to that observed for diverse cyanoferrate complexes bound to the titania surface.[63–66,74]

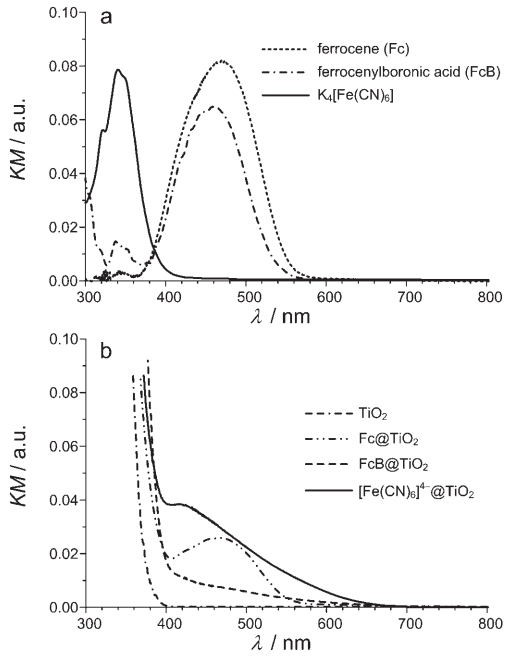

Figure 2. Transformed diffuse reflectance spectra of a) studied photosensitizers and b) titanium dioxide modified with corresponding iron complexes.

A completely new type of electronic transition appears after adsorption of hexacyanoferrate complex at TiO_2 surface. The broad band with maximum at 415 nm recorded for $[Fe(CN)_6]^{4-}$@TiO_2, which does not appear in the absorption spectrum of $[Fe(CN)_6]^{4-}$, is attributed to the MMCT transition, namely $Fe^{II} \rightarrow Ti^{IV}$.[61–72]

The described spectral features of all three materials are parallel to the semiconductor/surface-complex interaction. The interaction between ferrocene and titanium dioxide is very weak—slight spectral changes reflect a simple physisorption of the iron complex at the surface of TiO_2 with a very weak electronic coupling. Ferrocenylboronic acid binds chemically to the titania surface through a B-O-Ti framework, providing a platform for stronger electronic interactions. The appearance of this process is supported by spectral differences between ferrocenylboronic acid and the FcB@TiO_2 material. Formation of a new type of absorption observed for $[Fe(CN)_6]^{4-}$@TiO_2 indicates the strongest electronic coupling between the two electronic systems: isolated electronic levels of the complex and the electronic continuum of the semiconducting support. The MMCT nature of this new absorption band has been described in detail elsewhere.[61–72] The strength of the electronic coupling can be also deduced from the shape of the photosensitizer absorption bands. No significant changes in the energy and shape of electronic transitions within the photosensitizer indicate a lack of electronic coupling (Figure 3a). For electronically interacting systems the adsorbate (photosensitizer) bandwidth

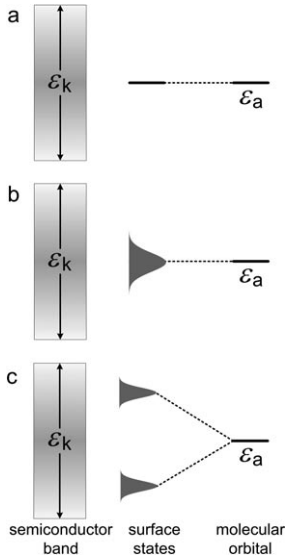

Figure 3. Energy diagrams for surface-modified semiconductors in the case of: a) no electronic coupling, b) weak electronic coupling, and c) strong electronic coupling.

broadening is associated with the degree of electronic coupling with the support according to Equation (4),[58] in which ε_k is the width of the semiconductor band.

$$\Gamma(E) = \pi \sum_k |V_{ET}(k)|^2 \delta(E-\varepsilon_k) \quad (4)$$

Equation (4) is valid for all the systems in which the bandwidth of the support is larger than the electron-transfer term V_{ET}. In this case, the energy level of the adsorbate is broadened into a resonance centered around ε_a (Figure 3b). In the case of a very strong coupling the absorbate state splits into bonding and antibonding states, both exhibiting strong broadening owing to the interaction with electronic continuum (Figure 3c).[58] Further evidence for energy-level broadening was observed in photoelectrochemical measurements (vide infra).

Postulated electronic coupling between electronic levels of adsorbates and electronic continuum of the semiconducting support does not significantly influence the electronic structure of the inner part of semiconductor particles. The indirect band-gap energy determined for neat titanium dioxide amounts 3.25 eV, which is consistent with the previously reported value. Interaction with any of the studied photosensitizers does not change the value for the neat material (Figure 4). In the case of zero electronic coupling no new bandlike spectral features are formed (Figure 4b). The ferrocene-related absorption can be described with a single Gaussian component. Mixing of occupied electronic levels of a photosensitizer with the conduction band of the semiconductor results in new transitions. Due to a significant broadening [cf. Eq. (4)], instead of typical (Gaussian-shape) absorption bands additional edge-type absorptions are observed (Figure 4c, d).

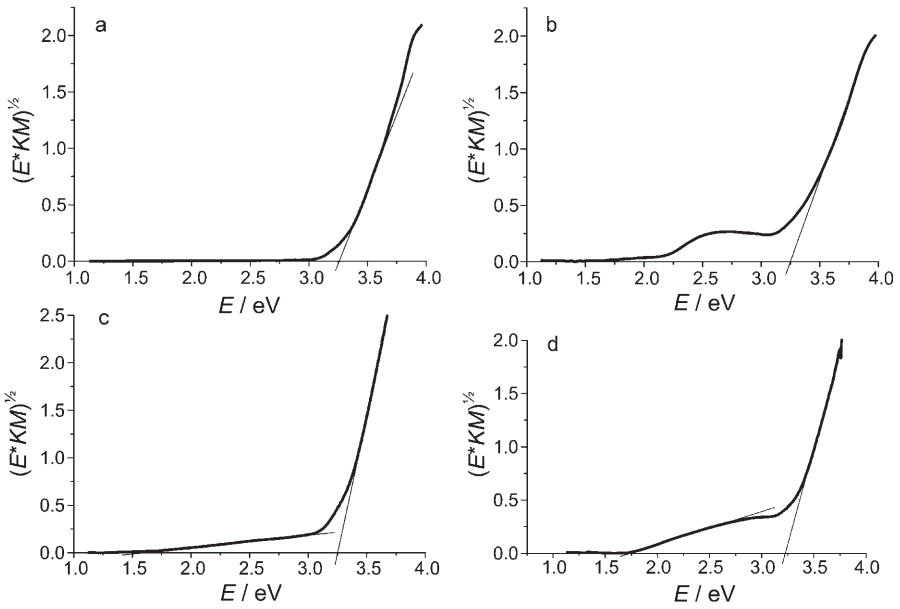

Figure 4. Determination of indirect band-gaps for a) neat titanium dioxide, b) Fc@TiO_2, c) FcB@TiO_2, and d) $[Fe(CN)_6]^{4-}$@TiO_2.

These new band gaps are associated with broadened surface states resulting from the photosensitizer–semiconductor interaction (cf. Figure 3b, c). These surface bands are characterized by 1.75 eV band-gap energies, in accordance to observed photosensitization of these materials (vide infra).

The interaction between the photosensitizer and the semiconducting support should influence the energy (or redox potentials) of the conduction- and valence-band edges. These data can be obtained from the quasi-Fermi level measurements[75,76] (i.e. the Fermi level potential measured for a semiconducting material under irradiation, E_{qF}), which together with the spectral characteristics of the synthesized materials allow the determination of the redox properties of the excited semiconducting materials. The modified method of the quasi-Fermi level determination,[75] described by Roy et al.,[76] was applied. This method bases on the pH-dependency of the valence- and conduction-bands edges potentials of the semiconductor particles. In the case of titanium dioxide with increasing pH the cathodic shift of E_{qF} by 59 mV per one pH unit was reported[75,76] [$k = -0.059$ V, Eq. (5)].

$$E_{qF} = E^0 + k(pH_0 - pH) \quad (5)$$

In combination with a pH-independent reversible redox pair (for instance a compound from the group of viologens) the electrons from the conduction band of the irradiated semiconductor may or may not reduce the redox couple, depending on the pH value and relative potentials (Figure 5). At pH values lower than pH_0 (i.e. pH value of potential lines crossing) the photoinduced reduction of the redox couple does not take place. This process is, however, possible in more basic media. Therefore the measurement of the E_{qF} is obtained from the determination of the pH_0 value.

The measured pH_0 (Figure 6), that is, pH values at which the quasi-Fermi level potential equilibrates with the redox potential of the methylviologen^{2+}/methylviologen$^{\bullet+}$ couple, enable calculation of the quasi-Fermi level potentials. Ferrocene and ferrocenylboronic acid almost do not influence the quasi-Fermi level potential, which remains very similar to that measured for neat TiO_2 (P25) material. At pH 7 they are about −0.62, −0.60, and −0.58 V (vs. NHE) for Fc@TiO_2, FcB@TiO_2, and P25, respectively. A significant anodic shift of the bands edges can be observed only in the case of $[Fe(CN)_6]^{4-}$@TiO_2 material (−0.47 V at pH 7), for which the photosensitizer–support electronic interaction is the most efficient (vide supra). The observed shift is, however,

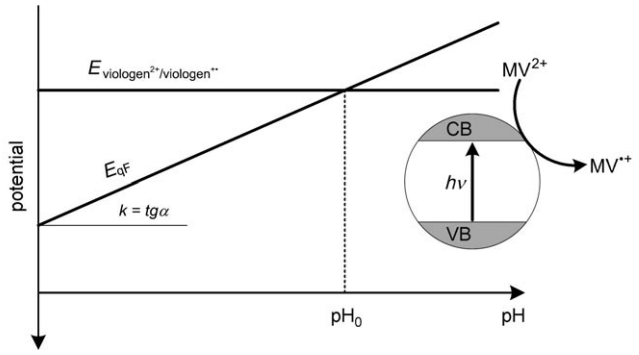

Figure 5. A principle of the quasi-Fermi level potential measurement.

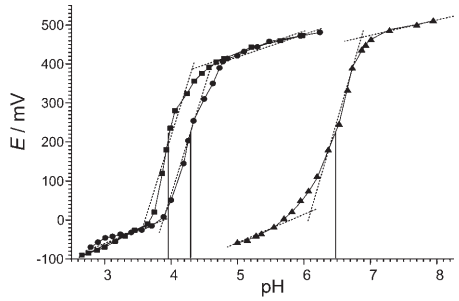

Figure 6. Titration curves and found pH_0 values for $Fc@TiO_2$ (squares), $FcB@TiO_2$ (circles), and $[Fe(CN)_6]^{4-}@TiO_2$ (triangles).

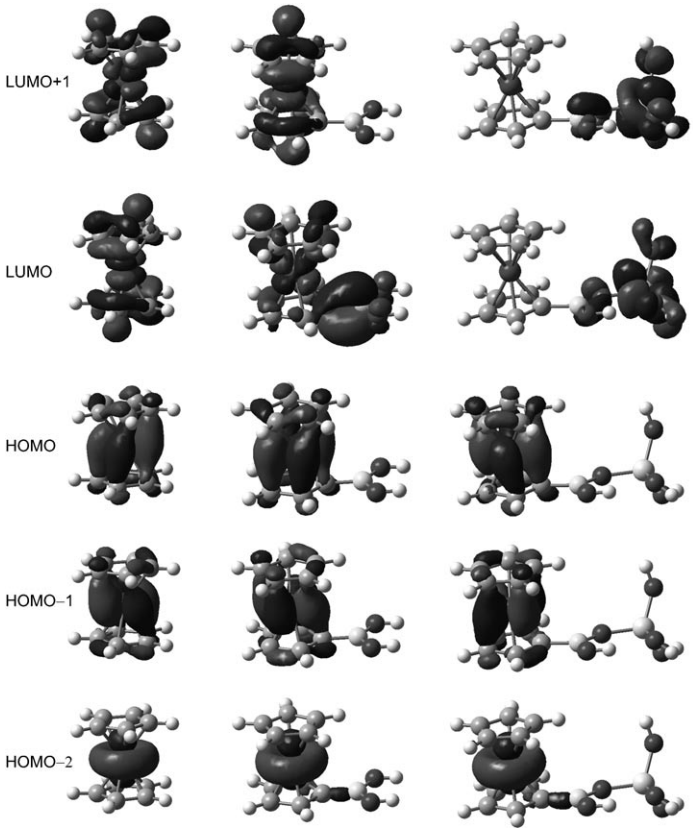

Figure 7. Frontier molecular orbitals of a) ferrocene, b) ferrocenylboronic acid and c) ferrocenylboronatetrihydroxytitanium(IV) as calculated at the B3PW91/6–311++G(d,p) level of theory by using tight convergence criteria.

mainly a result of the negative charge of the surface cyanoferrate complex.

Quantum-chemical modeling: Bonding of ferrocenylboronic acid and hexacyanoferrate(II) to the titanium centers of TiO_2 surface was modeled by using simple binuclear model complexes: $[(C_5H_5)Fe(C_5H_4)B(OH)OTi(OH)_3]$ and $[(CN)_5Fe{-}C{\equiv}N{-}Ti(OH)_3]^{3-}$, respectively. One Ti^{IV} ion with three hydroxide ligands, $\{\text{-}Ti(OH)_3\}^+$, was used as a simplified model of titanium dioxide surface. Although very simple, the models can reproduce all the bonding modes between the semiconductor surface and metal complexes.[66,70,72] The $\{\text{-}Ti(OH)_3\}^+$ moiety was chosen instead of $\{\text{-}Ti(OH)_5\}^-$ in order to eliminate the electrostatic repulsion between the metal centers in the case of the cyanoferrate counterpart.

Binding of the ferrocenylboronic acid to the surface of titanium dioxide most probably involves formation of a single B-O-Ti bridge. Bonding through two bridges with concomitant formation of the six-membered chelate ring is also possible, but according to DFT calculations is less favored. Interaction with titanium center does not induce any geometrical changes within the ferrocene moiety, but significantly changes its electronic structure (Figure 7).

The filled molecular orbitals of all the three ferrocene species are very similar: the HOMO−2 orbital consists mostly of d_{z^2} orbital of the iron center, while the HOMO−1 and HOMO orbitals, with π bonding character, are linear combinations of p_z orbitals of carbon atoms. The LUMO and LUMO+1 orbitals of ferrocene consist of d_{xz} and d_{yz} orbitals of the iron atom and the p_x and p_y orbitals of carbon atoms. In the case of ferrocenylboronic acid the LUMO contains a significant contribution of boron and oxygen atomic orbitals from the boronic acid moiety. The most significant changes of LUMO orbitals were observed in the case of titanium complexes with ferrocenylboronic acid: they are composed of d orbitals of titanium atom with a small admixture of oxygen atom orbitals. These changes are responsible for different spectral properties of the free ferrocenylboronic acid and the corresponding titanium compound.

The hexacyanoferrate system yielded the results analogous to those obtained for pentacyanoferrate model species[66,70] and Prussian blue,[72] and are consistent with previous calculations on TiO_2 nanoparticles modified with hexacyanoferrate(II).[65] The HOMO of the hexacyanoferrate(II) consists of threefold degenerate molecular orbitals composed mostly of the p orbitals of nitrogen atoms and d orbitals of iron atoms. The threefold degenerate LUMO is delocalized over the whole complex anion (Figure 8a). Upon interaction with the titanium center new species are formed due to formation of the Fe−C≡N−Ti bonding framework.

The HOMO−1 and HOMO orbitals are localized at iron(II) center, while the LUMO and LUMO+1 orbitals at the titanium center (Figure 8b). This electronic configura-

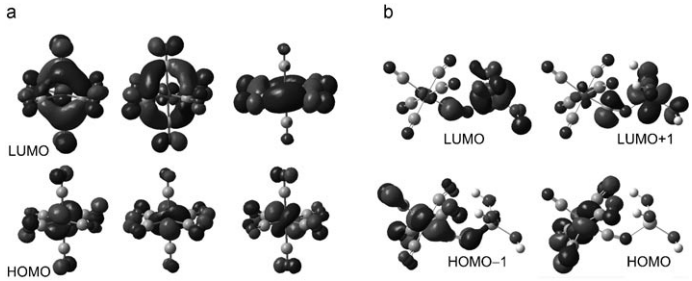

Figure 8. Frontier molecular orbitals of a) the $[Fe(CN)_6]^{4-}$ ion and b) the $[(CN)_5Fe\text{-}C{\equiv}N\text{-}Ti(OH)_3]^{3-}$ model compound as calculated at the B3PW91/6–311++G(d,p) level of theory by using tight convergence criteria.

tion clearly explains observed MMCT transitions, as low-energy transitions result in the electron transfer from the cyanoferrate moiety towards the titanium center.

Photoelectrochemical properties: Various types of electronic interaction between the iron complex and semiconducting support (TiO_2) reflect in different photoelectrochemical behaviors of tested systems. The measurements of photocurrent generated upon monochromatic-light irradiation at electrodes made of $[Fe(CN)_6]^{4-}$@TiO_2 were described elsewhere.[68,70,72]

Linear-sweep voltammetry (Figure 9) indicates an important role of oxygen and redox processes involving surface complexes in the mechanism of photocurrent generation.

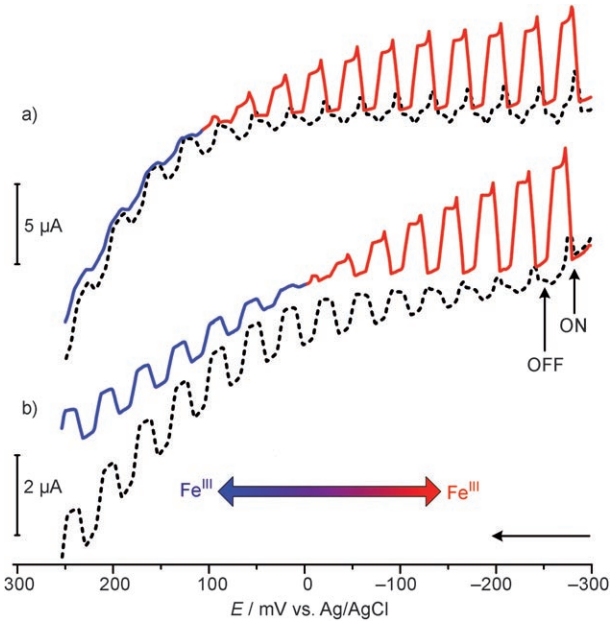

Figure 9. Linear sweep voltammograms recorded during chopped light illumination (350 nm) of a) Fc@TiO_2 and b) FcB@TiO_2 photoelectrodes in the presence (solid line) and absence of oxygen (dashed line). Vertical arrows indicate the opening and closing the shutter, respectively, while the horizontal arrow indicates the scan direction. Red and blue lines correspond to cathodic and anodic photocurrent, respectively. Fe^{II} and Fe^{III} indicate dominating oxidation states of the surface complex.

Downward deflection of the voltamperometric curves with increasing potential indicates the oxidation of Fe^{II} complexes on the surface of the semiconductor particles. Under such conditions only anodic photocurrents are observed. Cathodic photocurrents are recorded only in the presence of oxygen at sufficiently low potentials enabling complete reduction of surface iron species. Photocathodic response can be observed for photoelectrodes made of titanium dioxide modified with ferrocene and ferrocenylboronic acid at potentials lower than approximately 100 and 0 mV vs. Ag/AgCl, respectively (Figure 9). In the absence of oxygen only small anodic photocurrents are observed under similar conditions. The cathodic photocurrent can be generated at moderately low potentials only when the iron surface complex is present in its reduced form and in the presence of an efficient acceptor of electrons from the conduction band of modified titania.[68,70,72] A relatively high cathodic photocurrents were observed for the Fc@TiO_2 electrode (Figure 9). It may be explained by a highly hydrophobic surface of this material at which the photoinduced reduction of adsorbed hydrophobic oxygen molecules is particularly efficient. Surface complexes formed by ferrocenylboronic acid and hexacyanoferrate are much more hydrophilic.

Each material has been subjected for studies of photocurrent generation as a function of the electrode potential and applied photon energy. Recorded 3D diagrams are presented in Figure 10.

Unmodified titanium dioxide generates anodic photocurrent within a wide potential window upon UV illumination. At very high negative polarization cathodic photocurrents are observed due to reduction of some surface Ti^{IV} centers to Ti^{III} (Figure 10a), while the other materials generate cathodic photocurrent even at anodic polarization (Figure 10b–d). An interesting difference between Fc@TiO_2 and FcB@TiO_2 materials is reflected in photocurrent switching characteristics observed for the electrodes made of these materials. In the case of titania modified with ferrocene, a cathodic to anodic photocurrent switching in oxygen-saturated electrolyte appears within a very narrow potential range, namely from 100 to 150 mV vs. Ag/AgCl. Analogous switching observed for the FcB@TiO_2 photoelectrode takes place in the twice as broad potential range: from 0 to 100 mV. The photocurrent switching for the $[Fe(CN)_6]^{4-}$@TiO_2 material occurs between −130 and 260 mV. In all the cases the potential of the photocurrent switching depends on the incident light wavelength. This phenomenon can be easily explained in terms of electronic-level broadening (cf. Figure 3). In all the cases switching is related to the redox process involving the surface species.

In the case of ferrocene it undergoes a rather undisturbed redox reaction and the influence of semiconducting surface is negligible. Therefore the switching is very sharp (cf. Figure 10). In the case of ferrocenylboronic acid, in contrast to physisorbed ferrocene, various types of surface species may be formed, which corresponds to the decrease of electronic levels degeneration and formation of a narrow band-like energetic structure (cf. Figure 3b). A covalently linked

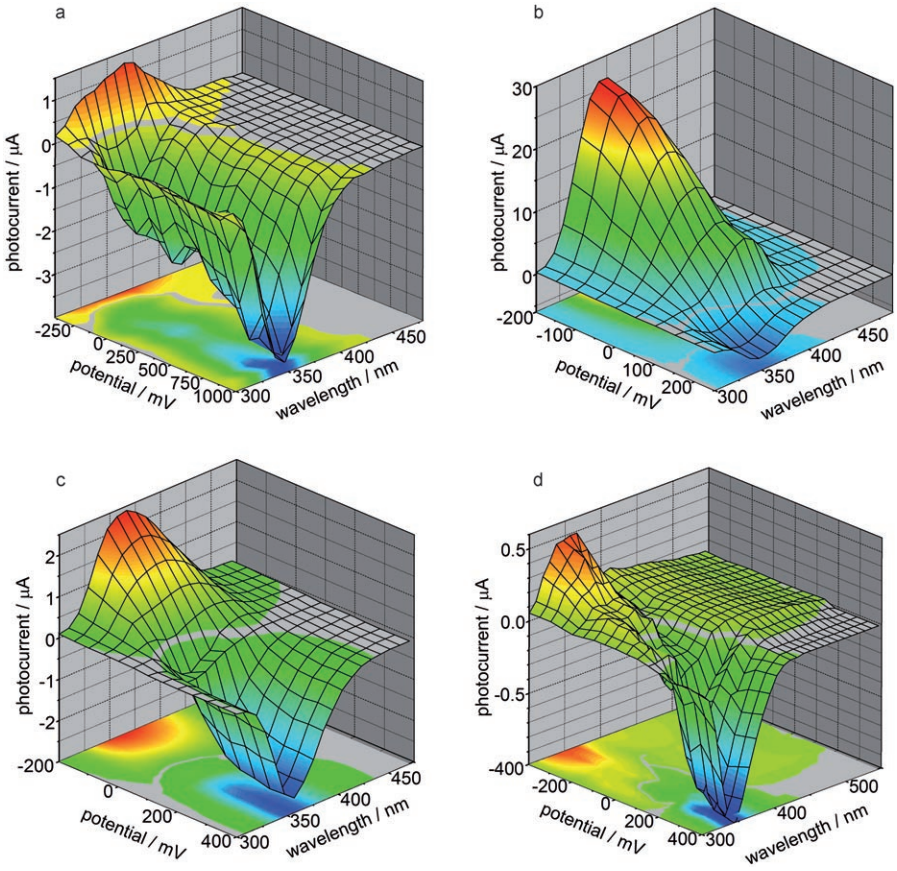

Figure 10. Photocurrent amplitude as a function of the photoelectrode potential and incident light wavelength recorded for photoelectrodes made of: a) TiO_2, b) Fc@TiO_2, c) FcB@TiO_2, and d) $[Fe(CN)_6]^{4-}$@TiO_2. Red and blue areas correspond to cathodic and anodic photocurrent, respectively, while gray areas represent zero net photocurrent.

iron species together with simply adsorbed organometallic moieties support centers of slightly different redox potentials. Therefore a complete reduction of iron complexes takes place in a broader range of potentials. This in turn results in a more fuzzy photocurrent switching observed in the case of FcB@TiO_2. In the strong coupling regime (cf. Figure 3c) observed for example for the $[Fe(CN)_6]^{4-}$@TiO_2 material a wide distribution of redox potentials of the surface complex is observed. Therefore the photocurrent switching can be observed in a wide range of potentials.

Furthermore, some minor issues may be associated with the sharpness (or fuzziness) of the photocurrent switching phenomenon. Photocurrent generation in the cathodic regime relies on molecular oxygen (or other electron acceptor) availability. Therefore application of a strongly hydrophobic layer on TiO_2 particles greatly enhances the local oxygen concentration, which results in anomalously high intensities of cathodic photocurrents at Fc@TiO_2 photoelectrodes.

Photosensitization mechanism: Photocurrent action spectra from Figure 10 confirm photosensitization of the titania support by iron complexes in the range of cathodic photocurrents. A slight photosensitization, extending the photoresponse to about 450 nm, can be observed for TiO_2 modified with ferrocene. Covalently linked ferrocenylboronic acid causes a more pronounced effect—the cathodic photocurrents are generated upon irradiation up to 550 nm. In the case of hexacyanoferrate complex attached to the titanium dioxide surface through the CN^- bridges the onset of the photoaction spectrum is localized at even longer wavelengths ($\approx$650 nm). All applied iron complexes can act as photosensitizers only in their reduced forms. At electrode potentials high enough to oxidize the surface complex, anodic photocurrents are recorded due to a direct excitation of TiO_2 with ultraviolet light.

To understand the photosensitization of titanium dioxide with ferrocenylboronic acid the absorption spectrum of the $[(C_5H_5)Fe\text{-}(C_5H_4)B(OH)OTi(OH)_3]$ model compound was calculated by using the time-dependent DFT methods at the B3PW91/6–311++G(d,p) level. The low-energy transition is found at 557 nm and has a mixed character: charge transfer ($\pi \rightarrow Ti^{IV}$, HOMO$\rightarrow$LUMO) together with the $d_{z^2} \rightarrow \pi^*$ and $\pi \rightarrow \pi^*$ transitions (within the ferrocene moiety). It leads to the conclusion that excitation of the FcB-modified titanium dioxide results in a direct photoinduced electron transfer from the ferrocene moiety to the conduction band of TiO_2. This hypothesis was further tested in calculation of the charge distribution of the ground and first-excited states of the model complex. It was found that upon excitation the titanium center becomes significantly negative, while the ferrocene moiety gains a positive character (Figure 11). Similar results were obtained for cyanoferrate with attached trihydroxotitanium(IV) moiety.[66]

Comparison of photoaction spectra with electronic spectra of studied photomaterials (Figure 10 and Figure 2) indicates, that observed photosensitization effect, increasing in the series Fc@TiO_2 < FcB@TiO_2 < $[Fe(CN)_6]^{4-}$@TiO_2, is not related exclusively to the absorption spectrum of the surface complex, but is a consequence of efficiency of the electron injection from the excited state of Fe^{II} species to the conduction band of the semiconductor. The above-mentioned series meets with the influence of the surface complex on the shift of redox potentials of bands edges: the anodic shift

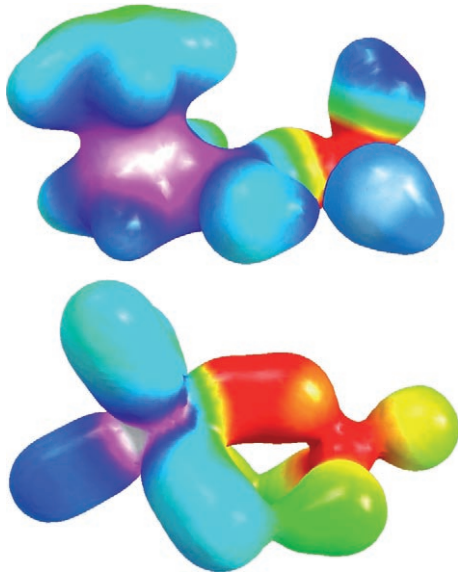

Figure 11. Change of electrostatic potential upon excitation to the first excited state of a) the $[(C_5H_5)Fe(C_5H_4)B(OH)OTi(OH)_3]$ and b) $[(CN)_5Fe\text{-}C{\equiv}N\text{-}Ti(OH)_3]^{3-}$ model compounds as calculated on the B3PW91/6–311++G(d,p) level of theory using tight convergence criteria. Areas of negative and positive potentials are marked in red and pinkish-white, respectively.

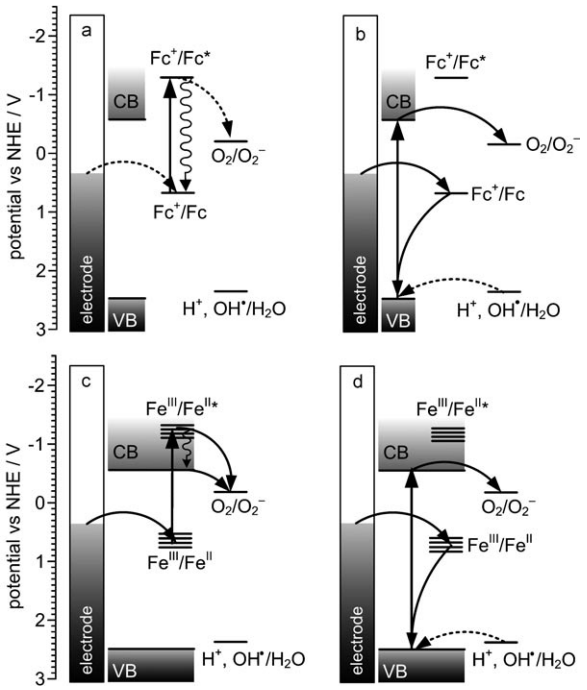

Figure 12. The mechanism of the cathodic photocurrent generation at a),b) the Fc@TiO_2-covered electrode and at c),d) $[Fe(CN)_6]^{4-}$@TiO_2-covered electrode.

of the quasi-Fermi level caused by hexacyanoferrate ion is very distinctive, while for FcB@TiO_2 and Fc@TiO_2 it is negligible.

Photoswitching mechanism: The photocurrent switching effect, called the PEPS effect (PhotoElectrochemical Photocurrent Switching) was described in our recent papers.[66–72]

Since photosensitization of titanium dioxide by ferrocene is very ineffective, photocurrents generated at the Fc@TiO_2 electrode upon visible-light irradiation are very poor and also the photocurrent switching upon changing the light wavelength is almost negligible (Figure 12a). There is no electronic interaction between the semiconductor and the surface complex, a very weak photocathodic response originates from processes involving only ferrocene molecules. This is supported by observation of similar cathodic photocurrents on photoelectrodes made of Fc@Al_2O_3 composite. Cathodic low intensity photocurrents recorded within the whole absorption spectrum of $[Fe(C_5H_5)_2]$ indicate that ferrocene behaves like a weak p-type semiconductor. Illumination within the semiconductor absorption at potentials higher than 100 mV results in anodic photocurrents according to generally accepted mechanism.[77,78] At potentials lower than 100 mV an unusual increase of cathodic photocurrent results from oxidation of ferrocene with photogenerated holes in the valence band (Figure 12b). This process is followed by consecutive electrochemical reduction of generated ferricinium cations. In addition, better oxygen adsorption at highly hydrophobic ferrocene-coated surface enhances the efficiency of interfacial electron transfer.[79] The material can be regarded as a bulk p–n heterojunction, which is consistent with recorded very high cathodic photocurrent intensities.[80–83] Formation of the p–n bulk heterojunctions in photovoltaic devices is an advantageous feature. It minimizes the charge recombination and thus increases the photocurrent intensities.[81]

In contrast to the Fc@TiO_2 system, the $[Fe(CN)_6]^{4-}$@TiO_2 material shows an efficient photosensitization (Figure 12c). Excitation of the reduced form of the iron species leads to a direct electron injection into the CB of the semiconductor. Reduction of oxygen and electrochemical regeneration of Fe^{II} leads to a cathodic photocurrent.[66,68,70] Direct excitation of the semiconductor results in a cathodic photocurrent due to the processes analogous to those described above (Figure 12d). Lower efficiencies of interfacial electron transfer are a consequence of worse oxygen adsorption at more hydrophilic surface.

The mechanism of photocurrent generation at FcB@TiO_2 is similar to that valid for Fc@TiO_2. Some photosensitization results from electron-transfer processes between the Fe^{II} and Ti^{IV} centers, which takes place with relatively low efficiency. Lower intensity of cathodic photocurrent results from higher hydrophilicity of ferrocenylboronic acid as compared to unsubstituted ferrocene.

In the case of both FcB@TiO_2 and $[Fe(CN)_6]^{4-}$@TiO_2 the cathodic photocurrent generation at low potentials under visible light irradiation is a result of the MPCT excitation followed by the oxygen reduction and electrochemical reduction of formed iron(III) complex. The difference between the FcB@TiO_2 and $[Fe(CN)_6]^{4-}$@TiO_2 materials is related to various efficiencies of the metal-to-particle charge

transfer resulting from different degree of electronic coupling, as confirmed by quantum-mechanical calculations (vide supra).

Future prospects: Switching properties of photoelectrodes comprised of surface-modified titanium dioxide can be used for construction of various prototypical optoelectronic devices.[68,69,71,72] The best example of a complex device originating from simple materials is a reconfigurable logic device built from cyanoferrate-modified titanium dioxide.[69,71]

The ferrocene-based materials generate photocurrent only upon UV and blue irradiation (300–450 nm), but the photocurrent character depends on the photoelectrode potential. In the case of ferrocene and ferrocenylboronate-modified materials the cathodic-to-anodic switching occurs in the range 100–150 mV and 0–100 mV vs. Ag/AgCl, respectively. At potentials higher than the switching potential range, the electrodes generate anodic photocurrent, while at lower potentials cathodic photocurrents are observed. One can assign the logic values of "0" and "1" to the negative and the positive polarization of the photoelectrode, respectively. The switching characteristics allow its use as an optoelectronic two channel demultiplexer (data selector). This device collects information in form of light pulses and converts it into photocurrent pulses. Furthermore, the sign (direction) of photocurrent pulses depends on the photoelectrode potential. In other words, information in form of photocurrent pulses can be directed into two output channels: cathodic or anodic. An electronic equivalent of this logic device is composed of two AND and NOT logic gates (Figure 13). The input data signal (light pulses) is applied to

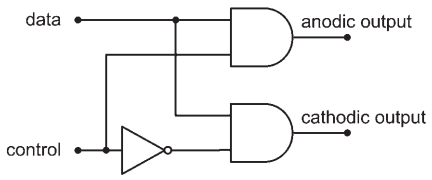

Figure 13. Electronic equivalent circuit of surface-modified titania photoelectrode working as two channel optoelectronic demultiplexer.

one input of both AND gates, the control signal goes to one AND gate directly, while it goes to the other via an inverter. In this configuration one of the AND gates is in the ON and the other in the OFF state (Table 1).

Thus, a signal applied to the data input is always transmitted by one of the AND gates and thus directed into one of the output channels. It is easy to imagine an application of similar systems in telecommunication. Nowadays information transmitted through optical fibers must be converted into electric signals and directed to the destination points. The Fc@TiO_2 and FcB@TiO_2 systems can serve as a simple chemical model of two channel demultiplexer. This is an interesting example of a simple chemical system working like a complex electronic circuit consisting of three logic elements.

Table 1. Truth table for the two channel demultiplexer presented in Figure 13.

Data	Control	Anodic Output	Cathodic Output
0	0	0	0
1	0	0	1
0	1	0	0
1	1	1	0

The above examples show that the nanocrystalline titanium dioxide modified with various iron complexes are promising materials for optoelectronics. Although very simple from chemical point of view, they offer complex switching patterns resulting from their rich photoelectrochemistry. The most interesting feature of these materials consists in the complexity of electronic functions (cf. Figure 13) contrasted with very simple morphology—unstructured deposits of nanocrystalline powders show properties equivalent to complex circuits. Related materials may open a new field of nanoelectronics; instead of a complex circuitry it may be enough to design a proper unstructured material of desired performance.

Conclusion

The results presented above indicate an important role of binding mode and resulting electronic interactions between surface species and semiconducting support. This information helps us to understand the mechanism of photosensitization and photocurrent switching, which can find an application in optoelectronics and photovoltaics. A series of titanium dioxide materials with various iron(II) complexes has been prepared. These materials are characterized by increasing electronic interaction between surface iron species and the semiconductor particles in the series: Fc@TiO_2 < FcB@TiO_2 < $[Fe(CN)_6]^{4-}$@TiO_2. In the same series the photosensitization range increases, from almost negligible for ferrocene-modified TiO_2 to very evident for cyanoferrate-modified semiconductor. These differences correlate well with estimated electronic interactions and are supported by calculated frontier orbitals and electronic spectra of model species. In the case of materials with covalently bonded, surface iron(II) species, a direct photosensitization of the semiconductor is observed [cf. Eq (3)]. This process includes a direct electron transfer from iron complexes to the conduction band of semiconductor. On the basis of theoretical analysis one can conclude that efficient photocurrent switching requires a subtle interplay between the $\hat{V}_{RMS}$ and $\hat{V}_{ET}$ components of the total Hamiltonian $\hat{H}$ [cf. Eqs. (1)–(3)]. The $\hat{V}_{RMS}$ term, responsible for the efficiency of photosensitization, can be correlated with the binding mode between the semiconductor and the surface species, while the $\hat{V}_{ET}$ component governs the electron-transfer processes that are responsible for photocurrent inversion.

On the other hand formation of p–n bulk heterojunction results in dramatic increase of photocurrent with a negligi-

ble photosensitization. All these heterosupramolecular assemblies in which metal complexes interact with semiconductor nanoparticles seem to be a promising area for photovoltaic and optoelectronic devices.

Experimental Section

Materials: TiO_2 (Degussa P25, ca. 70% anatase, 30% rutile; 50 $m^2 g^{-1}$) was used to prepare porous electrodes. All other chemicals were supplied by Aldrich and used as received. Titania–ferrocene nanocomposites were prepared as follows: TiO_2 (100 mg) and ferrocene (50 mg) were suspended in a mixture of acetonitrile and ethanol (1:1 v/v 2 cm^3). The resulting mixture was ground in an agate mortar until it became completely dry, was then suspended in water and was used for cast coating of ITO-covered glass slides. The same procedure was used to prepare Fc@$BaSO_4$ and Fc@Al_2O_3 composites used as reference materials. Cyanoferrate-modified titanium dioxide was obtained by impregnation of the TiO_2 powder in aqueous $K_4[Fe(CN)_6]$ solution (0.01 M) for 15 minutes. Modification with ferrocenylboronate was done in a solution of ferrocenylboronic acid in acetonitrile (0.01 M). After modification all materials were centrifuged, were washed five times with distilled water or acetonitrile, and were air-dried at room temperature. After preparation the modified semiconductor powders were stored in dark at 4 °C.

Instrumentation: The typical three-electrode set-up was employed for photoelectrochemical measurements. The electrolyte solution was 0.1 M KNO_3, which was purged with argon or oxygen for at least 15 min prior to the measurement. Platinum and Ag/AgCl were used as auxiliary and reference electrodes, respectively. A 150 W XBO lamp (Osram, Germany) equipped with water cooled housing and LPS 200 power supply (Photon Technology International, UK) was used for irradiation. The working electrodes were irradiated from the backside (through the ITO-glass) in order to minimize the influence of thickness of the semiconductor layer on the photocurrent values. An automatically controlled monochromator and a shutter were applied to choose the appropriate wavelength. Photocurrent action spectra were recorded under potentiostatic conditions and are not corrected for changes in light intensity. The electrochemical measurements (CV, CV + chopped light, photocurrent action spectra) were controlled by a BAS 50W (Bioanalytical Systems, USA) or M161 (MTM, Poland) electrochemical analyzers. Cyclic voltammograms were recorded with 25 mV s^{-1} scan rate.

Diffuse reflectance spectra were recorded on Lambda 12 (Perkin Elmer, USA) spectrophotometer equipped with an integrating sphere of 5 cm diameter. Barium sulfate was used as a reference material. The conduction-band edge potential was determined by using a modified Roy's procedure.[76] A sample of the semiconductor powder (40 mg) was suspended in aqueous potassium nitrate (0.1 M, 70 cm^3) and sonicated for 5 min. Methylviologen bis(hexafluorophosphate) (30 mg) was added and the resulting mixture was acidified with concentrated perchloric acid (1 cm^3). The suspension was placed in a rectangular glass vessel equipped with a combined pH electrode, platinum foil electrode (area 2.5 cm^2) and reference Ag/AgCl electrode (FLEXREF, World Precision Instruments, USA). The vessel was vigorously purged with argon and irradiated with full light of an HBO 200 mercury high pressure lamp. The solution was titrated with an aqueous solution of Na_2CO_3 (0.1 M) by using an infusion pump Medipan 610 B.S (Medipan, Poland) equipped with calibrated Hamilton syringes and a custom-build interface. The potential of the platinum electrode was measured by using BM-811 digital multimeter (Brymen, Taiwan).

Calculations: Theoretical modeling was performed with Gaussian 03 Rev. D.01 (Gaussian Inc.)[84] and ArgusLab 4.0.1 (Planaria Software, USA).[85] Preliminary geometry optimization was done with a molecular mechanics module[86–89] by using the UFF force field,[90–93] while the final geometry was obtained using DFT method with B3PW91 functional and 6–311++G(d,p) basis set. Atomic charges were computed by using NPO analysis. Molecular orbitals and surfaces were computed by using the same theory level and tight convergence criteria. Electronic transitions were calculated by using a time-dependent DFT method with B3PW91 functional and 6–311++G(d,p) basis set. Molecular orbitals and charge distribution diagrams were plotted from Gaussian cube files using ArgusLab 4.0.1 software.

Acknowledgements

Authors thank Mr. Radim Beranek for assistance during preparation of the manuscript. Financial support from Polish Ministry of Science and Higher Education (grants No. PB0941/T08/2005/28 and PBZ-KBN-118/T09/8) and Jagiellonian University is gratefully acknowledged. DFT calculations were performed in Academic Computer Centre CYFRONET AGH within computational grant No. MNiI/SGI ONYX/UJ/031/2005.

[1] L. M. Peter, K. G. U. Wijayantha, D. J. Riley, J. P. Waggett, *J. Phys. Chem. B* **2003**, *107*, 8378.
[2] X. Qian, D. Qin, Y. Bai, T. Li, X. Tang, E. Wang, S. Dong, *J. Solid State Electrochem.* **2001**, *5*, 562.
[3] R. Vogel, P. Hoyer, H. Weller, *J. Phys. Chem.* **1994**, *98*, 3183.
[4] S.-M. Yang, Z.-S. Wang, C.-H. Huang, *Synth. Met.* **2001**, *123*, 267.
[5] W. Ho, J. C. Yu, *J. Mol. Catal. A* **2006**, *247*, 268.
[6] M. S. Lee, S.-S. Hong, M. Mohseni, *J. Mol. Catal. A* **2005**, *242*, 135.
[7] J. C. Tristao, F. Magalhaes, P. Corio, M. T. C. Sansiviero, *J. Photochem. Photobiol. A* **2006**, *181*, 152.
[8] K. Yu, Y. Tian, T. Tatsuma, *Chem. Commun.* **2006**, 5417.
[9] Y. Tian, T. Tatsuma, *J. Am. Chem. Soc.* **2005**, *127*, 7632.
[10] T. Lana-Villareal, R. Gómez, *Electrochem. Commun.* **2005**, *7*, 1218.
[11] T. Lana-Villareal, R. Gómez, *Chem. Phys. Lett.* **2005**, *414*, 489.
[12] T. Sasaki, N. Koshizaki, J.-W. Yoon, K. M. Beck, *J. Photochem. Photobiol. A* **2001**, *145*, 11.
[13] C. He, X. Li, Y. Xiong, X. Zhu, S. Liu, *Chemosphere* **2005**, *58*, 381.
[14] R. Asahi, T. Morikawa, T. Ohwaki, K. Aoki, Y. Taga, *Science* **2001**, *293*, 269.
[15] T. Morikawa, R. Asahi, T. Ohwaki, K. Aoki, Y. Taga, *Jpn. J. Appl. Phys. Part 2* **2001**, *40*, L561.
[16] S. Sakthivel, H. Kisch, *ChemPhysChem* **2003**, *4*, 487.
[17] R. Silveyra, L. De La Torre Saénz, W. Antúnez Flores, V. C. Martínez, A. A. Elguézabal, *Catal. Today* **2005**, *107–108*, 602.
[18] C. Lettmann, K. Hildenbrand, H. Kisch, W. Macyk, W. F. Maier, *Appl. Catal. B* **2001**, *32*, 215.
[19] S. Sakthivel, H. Kisch, *Angew. Chem.* **2003**, *115*, 5057; *Angew. Chem. Int. Ed.* **2003**, *42*, 4908.
[20] T. Ohno, T. Tsubota, M. Toyofuku, R. Inaba, *Catal. Lett.* **2004**, *98*, 255.
[21] J. C. Yu, W. Ho, J. Yu, H. Yip, P. K. Wong, J. Zhao, *Environ. Sci. Technol.* **2005**, *39*, 1175.
[22] H. Luo, T. Takata, Y. Lee, J. Zhao, K. Domen, Y. S. Yan, *Chem. Mater.* **2004**, *16*, 846.
[23] X. Hong, Z. Wang, W. Cai, F. Lu, J. Zhang, Y. Yang, N. Ma, Y. Liu, *Chem. Mater.* **2005**, *17*, 1548.
[24] M. M. Rahman, K. M. Krishna, T. Soga, T. Jimbo, M. Umeno, *J. Phys. Chem. Solids* **1999**, *60*, 201.
[25] S. T. Martin, C. L. Morrison, M. R. Hoffmann, *J. Phys. Chem.* **1994**, *98*, 13695.
[26] M. Radecka, M. Wierzbicka, S. Komornicki, M. Rekas, *Physica B* **2004**, *348*, 160.
[27] D. Dvoranova, V. Brezova, M. Mazur, M. A. Malati, *Appl. Catal. B* **2002**, *37*, 91.
[28] L. Zang, W. Macyk, C. Lange, W. F. Maier, C. Antonius, D. Meissner, H. Kisch, *Chem. Eur. J.* **2000**, *6*, 379.
[29] W. Macyk, H. Kisch, *Chem. Eur. J.* **2001**, *7*, 1862.
[30] H. Kisch, G. Burgeth, W. Macyk, *Adv. Inorg. Chem.* **2004**, *56*, 241.
[31] G. Burgeth, H. Kisch, *Coord. Chem. Rev.* **2002**, *230*, 40.
[32] W. Macyk, G. Burgeth, H. Kisch, *Photochem. Photobiol. Sci.* **2003**, *2*, 322.

[33] K. T. Ranjit, I. Willner, S. H. Bossmann, A. M. Brauny, *J. Catal.* **2001**, *204*, 305.
[34] F. B. Li, X. Z. Li, M. F. Hou, K. W. Cheah, W. C. H. Choy, *Appl. Catal. A* **2005**, *285*, 181.
[35] Y. Xie, C. Yuan, *J. Chem. Technol. Biotechnol.* **2005**, *80*, 954.
[36] J. E. Kroeze, R. B. M. Koehorst, T. J. Savenije, *Adv. Funct. Mater.* **2004**, *14*, 992.
[37] J. H. Yu, J. R. Chen, X. S. Wang, B. W. Zhang, Y. Cao, *Chem. Commun.* **2003**, 1856.
[38] A. F. Nogueira, A. L. B. Formiga, H. Winnischofer, M. Nakamura, F. M. Engelmann, K. Araki, H. E. Toma, *Photochem. Photobiol. Sci.* **2004**, *3*, 56.
[39] A. F. Nogueira, L. F. O. Furtado, A. L. B. Formiga, M. Nakamura, K. Araki, H. E. Toma, *Inorg. Chem.* **2004**, *43*, 396.
[40] H. Winnischofer, A. L. B. Formiga, M. Nakamura, H. E. Toma, K. Araki, A. F. Nogueira, *Photochem. Photobiol. Sci.* **2005**, *4*, 359.
[41] C. Ingrosso, A. Petrella, M. L. Curri, M. Striccoli, P. Cosma, P. D. Cozzoli, A. Agostiano, *Appl. Surf. Sci.* **2005**, *246*, 367.
[42] V. Iliev, *J. Photochem. Photobiol. A* **2002**, 151, 195.
[43] S. Taira, T. Miki, H. Yanagi, *Appl. Surf. Sci.* **1999**, *143*, 23.
[44] H. Deng, H. Mao, Z. Lu, H. Xu, *Thin Solid Films* **1998**, *315*, 244.
[45] H. Deng, H. Mao, Z. Lu, H. Xu, *J. Photochem. Photobiol. A* **1997**, *110*, 47.
[46] A. Ehret, L. Stuhl, M. T. Spitler, *J. Phys. Chem. B* **2001**, *105*, 9960.
[47] S. Ushiroda, N. Ruzycki, Y. Lu, M. T. Spitler, B. A. Parkinson, *J. Am. Chem. Soc.* **2005**, *127*, 5158.
[48] R. Argazzi, N. Y. M. Iha, H. Zabri, F. Odobel, C. A. Bignozzi, *Coord. Chem. Rev.* **2004**, *248*, 1299.
[49] A. S. Polo, M. K. Itokazu, N. Y. M. Iha, *Coord. Chem. Rev.* **2004**, *248*, 1343.
[50] C. G. Garcia, A. S. Polo, N. Y. M. Iha, *J. Photochem. Photobiol. A* **2003**, *160*, 87.
[51] F. G. Gao, A. J. Bard, L. D. Kispert, *J. Photochem. Photobiol. A* **2000**, *130*, 49.
[52] J. Pan, G. Benkö, Y. Xu, T. Pascher, L. Sun, V. Sundström, T. Polívka, *J. Am. Chem. Soc.* **2002**, *124*, 13949.
[53] Y. Amao, T. Komori, *Biosens. Bioelectron.* **2004**, *19*, 843.
[54] J. Pan, Y. Xu, L. Sun, V. Sundström, T. Polivka, *J. Am. Chem. Soc.* **2004**, *126*, 3066.
[55] S. Hao, J. Wu, Y. Huang, J. Lin, *Solar Energy* **2006**, *80*, 209.
[56] Z. Zhou, S. Qian, S. Yao, Z. Zhang, *Radiat. Phys. Chem.* **2002**, *65*, 241.
[57] M. Galperin, A. Nitzan, *Phys. Rev. Lett.* **2005**, *95*, 206802.
[58] C. D. Lindstrom, X.-Y. Zhu, *Chem. Rev.* **2006**, *106*, 4281.
[59] M. Galperin, A. Nitzan, M. A. Ratner, *Phys. Rev. Lett.* **2006**, *96*, 166803.
[60] M. Galperin, A. Nitzan, *J. Chem. Phys.* **2006**, *124*, 234709.
[61] E. Vrachnou, M. Grätzel, A. J. McEvoy, *J. Electroanal. Chem. Interfacial Electrochem.* **1989**, *258*, 193.
[62] E. Vrachnou, N. Vlachopoulos, M. Grätzel, *J. Chem. Soc. Chem. Commun.* **1987**, 868.
[63] H. N. Gosh, J. B. Ashbury, Y. Weng, T. Lian, *J. Phys. Chem. B* **1998**, *102*, 10208.
[64] M. Khoudiakov, A. R. Parise, B. S. Brunschwig, *J. Am. Chem. Soc.* **2003**, *125*, 4637.
[65] F. De Angelis, A. Tilocca, A. Selloni, *J. Am. Chem. Soc.* **2004**, *126*, 15024.
[66] M. Hebda, G. Stochel, K. Szaciłowski, W. Macyk, *J. Phys. Chem. B* **2006**, *110*, 15275.
[67] K. Szaciłowski, W. Macyk, *Ann. Pol. Chim. Soc.* **2004**, *4*, 768.
[68] K. Szaciłowski, W. Macyk, *C. R. Chim.* **2006**, *9*, 315.
[69] K. Szaciłowski, W. Macyk, *Solid-State Electron.* **2006**, *50*, 1649.
[70] K. Szaciłowski, W. Macyk, M. Hebda, G. Stochel, *ChemPhysChem* **2006**, *7*, 2384.
[71] K. Szaciłowski, W. Macyk, G. Stochel, *J. Am. Chem. Soc.* **2006**, *128*, 4550.
[72] K. Szaciłowski, W. Macyk, G. Stochel, *J. Mater. Chem.* **2006**, *16*, 4603
[73] L. G. C. Rego, V. S. Batista, *J. Am. Chem. Soc.* **2003**, *125*, 7989.
[74] M. Yang, D. W. Thompson, G. J. Meyer, *Inorg. Chem.* **2000**, *39*, 3738.
[75] D. Duonghong, J. Ramsden, M. Grätzel, *J. Am. Chem. Soc.* **1982**, *104*, 2977.
[76] A. M. Roy, G. C. De, N. Sasmal, S. S. Bhattacharyya, *Int. J. Hydrogen Energy* **1995**, *20*, 627.
[77] J. J. Ramsden, R. Tóth-Boconádi, *J. Chem. Soc. Faraday Trans.* **1990**, *86*, 1527.
[78] K. Uosaki, H. Kita, in *Modern aspects of electrochemistry, Vol. 18* (Eds.: R. E. White, J. O. M. Bockris, B. E. Conway), Plenum, New York, **1986**.
[79] A. Jańczyk, E. Krakowska, G. Stochel, W. Macyk, *J. Am. Chem. Soc.* **2006**, *128*, 15574.
[80] A. D. Q. Li, L. S. Li, *J. Phys. Chem. B* **2004**, *108*, 12842.
[81] J. Bandara, U. W. Pradeep, R. G. S. J. Bandara, *J. Photochem. Photobiol. A* **2005**, *170*, 273.
[82] V. P. S. Perera, P. V. V. Jayaweera, P. K. D. D. P. Pitigala, P. K. M. Bandaranayake, G. Hastings, A. G. U. Perera, K. Tennakone, *Synth. Met.* **2004**, *143*, 283.
[83] M. Pientka, V. Dyakonov, D. Meissner, A. Rogach, D. Talapin, H. Weller, L. Lutsen, D. Vanderzande, *Nanotechnology* **2004**, *15*, 163.
[84] Gaussian 03, Revision D.01, M. J. Frisch, G. W. Trucks, H. B. Schlegel, G. E. Scuseria, M. A. Robb, J. R. Cheeseman, J. A. Montgomery, Jr., T. Vreven, K. N. Kudin, J. C. Burant, J. M. Millam, S. S. Iyengar, J. Tomasi, V. Barone, B. Mennucci, M. Cossi, G. Scalmani, N. Rega, G. A. Petersson, H. Nakatsuji, M. Hada, M. Ehara, K. Toyota, R. Fukuda, J. Hasegawa, M. Ishida, T. Nakajima, Y. Honda, O. Kitao, H. Nakai, M. Klene, X. Li, J. E. Knox, H. P. Hratchian, J. B. Cross, V. Bakken, C. Adamo, J. Jaramillo, R. Gomperts, R. E. Stratmann, O. Yazyev, A. J. Austin, R. Cammi, C. Pomelli, J. W. Ochterski, P. Y. Ayala, K. Morokuma, G. A. Voth, P. Salvador, J. J. Dannenberg, V. G. Zakrzewski, S. Dapprich, A. D. Daniels, M. C. Strain, O. Farkas, D. K. Malick, A. D. Rabuck, K. Raghavachari, J. B. Foresman, J. V. Ortiz, Q. Cui, A. G. Baboul, S. Clifford, J. Cioslowski, B. B. Stefanov, G. Liu, A. Liashenko, P. Piskorz, I. Komaromi, R. L. Martin, D. J. Fox, T. Keith, M. A. Al-Laham, C. Y. Peng, A. Nanayakkara, M. Challacombe, P. M. W. Gill, B. Johnson, W. Chen, M. W. Wong, C. Gonzalez, J. A. Pople, Gaussian, Inc., Wallingford CT, **2004**.
[85] M. A. Thompson, ArgusLab 4.0, Planaria Software LLC, Seattle, WA (http://www.arguslab.com) **2004**.
[86] M. A. Thompson, M. C. Zerner, *J. Am. Chem. Soc.* **1991**, *113*, 8210.
[87] M. A. Thompson, E. D. Glendening, D. Feller, *J. Phys. Chem.* **1994**, *98*, 10465.
[88] M. A. Thompson, G. K. Schenter, *J. Phys. Chem.* **1995**, *99*, 6374.
[89] M. A. Thompson, *J. Phys. Chem.* **1996**, *100*, 14492.
[90] C. J. Casewit, K. S. Colwell, A. K. Rappe, *J. Am. Chem. Soc.* **1992**, *114*, 10035.
[91] C. J. Casewit, K. S. Colwell, A. K. Rappe, *J. Am. Chem. Soc.* **1992**, *114*, 10046.
[92] A. K. Rappe, W. A. Goddard, *J. Phys. Chem.* **1991**, *95*, 3358.
[93] A. K. Rappe, K. S. Colwell, C. J. Casewit, *Inorg. Chem.* **1993**, *32*, 3438.

Received: February 7, 2007
Published online: May 30, 2007

